DREDGE-UP AND ENVELOPE BURNING IN INTERMEDIATE-MASS GIANTS OF VERY LOW METALLICITY

FALK HERWIG

Department of Physics and Astronomy, University of Victoria, 3800 Finnerty Road, Victoria, BC V8P 1A1, Canada; and
Los Alamos National Laboratories, Los Alamos, NM 87544; fherwig@lanl.gov
Received 2003 July 3; accepted 2003 December 22

ABSTRACT

The evolution of intermediate-mass stars at very low metallicity during their final thermal pulse asymptotic giant branch (AGB) phase is studied in detail. As representative examples, models with initial masses of 4 and 5 $M_\odot$ and with a metallicity of $Z = 0.0001$ ([Fe/H] ~ -2.3) are discussed. The one-dimensional stellar structure and evolution model includes time- and depth-dependent overshooting motivated by hydrodynamic simulations, as well as a full nuclear network and time-dependent mixing. Particular attention is given to high time and space resolution to avoid numerical artifacts related to third dredge-up and hot bottom burning predictions. The model calculations predict very efficient third dredge-up that mixes the envelope with the entire intershell layer or a large fraction thereof and in some cases penetrates into the C/O core below the He shell. In all cases primary oxygen is mixed into the envelope. The models predict efficient envelope burning during the interpulse phase. Depending on the envelope-burning temperature, oxygen is destroyed to varying degrees. The combined effect of dredge-up and envelope burning does not lead to any significant oxygen depletion in any of the cases considered in this study. The large dredge-up efficiency in our model is closely related to the particular properties of the H shell during the dredge-up phase in low-metallicity very metal-poor stars, which is followed here over many thermal pulses. During the dredge-up phase, the temperature just below the convective boundary is large enough for protons to burn vigorously when they are brought into the C-rich environment below the convection boundary by the time- and depth-dependent overshooting. H-burning luminosities of 10^5 to $\sim 2 \times 10^6$ $L_\odot$ are generated. C, and to lesser degree O, is transformed into N in this dredge-up overshooting layer and enters the envelope. The global effect on the CNO abundance is similar to that of hot bottom burning. If the overshoot efficiency is larger, then dredge-up H burning causes a further increase in the dredge-up efficiency. After some thermal pulses, the dredge-up proceeds through the He shell and into the CO core beneath. Then neutrons may not be released from ^{13}C in radiative conditions during the interpulse phase because of the scarcity of α-particles for the ^{13}C$(\alpha, n)^{16}$O reactions. Conditions for the s-process are discussed qualitatively. The abundance evolution of H, He, C, N, O, and Na is described. Finally, the model predictions for sodium and oxygen are compared with observed abundances. The notion that massive AGB stars are the origin of the O-Na abundance anticorrelation in globular cluster giants is not consistent with the model predictions of this study. The abundance of the C-rich extremely metal-poor binaries LP 625-44, CS 29497-030, and HE 0024−2523 is discussed.

Subject headings: nuclear reactions, nucleosynthesis, abundances — stars: abundances —
stars: AGB and post-AGB — stars: evolution — stars: Population II

On-line material: color figure

1. INTRODUCTION

During their final evolutionary phase, intermediate-mass stars (IMSs) proceed through the thermal pulse asymptotic giant branch (TP-AGB) stage (e.g., Iben & Renzini 1983; Lattanzio & Forestini 1999; Herwig 2003). Hydrogen and helium is processed in distinct nuclear shells around the increasingly electron-degenerate CO core. Periodically, the He shell becomes unstable because of a combination of the well-known thin-shell instability and partial degeneracy. The thin-shell instability is a common feature in nuclear shells around degenerate cores and can be found in accreting white dwarfs (novae) and He-core white dwarfs, as well as in accreting neutron stars (X-ray bursts). In AGB stars the He-shell flash causes a complicated series of mixing events, including a pulse-driven convection zone (PDCZ) that comprises the entire intershell layer. These mixing events eventually lead to a significant envelope abundance enrichment with material processed by either or both the He shell and the H shell.

In the past, most AGB stellar evolution calculations were carried out for the solar metallicity, moderate metal deficiency, or zero metallicity (e.g., Karakas, Lattanzio, & Pols 2002; Siess, Livio, & Lattanzio 2002). However, there are a number of reasons to study the evolution of AGB stars at very low nonzero metallicity ($0.0 < Z \leq 0.0001$). For example, recent observations of ^{14}N in metal-poor stars and, in particular, in the damped Lyα absorbers (Pettini et al. 2002; Prochaska et al. 2002) have sparked a debate on whether the results are to be interpreted as a primary origin of ^{14}N in IMSs or as a result of a peculiar (top-heavy) initial mass function at very low metallicity.

Detailed abundance studies of extremely metal-poor (EMP) carbon-rich stars are now reported in increasing numbers (e.g., Lucatello et al. 2003; Aoki et al. 2002a). Many of these carbon-rich EMP stars are nitrogen-rich as well, and often—when it has been determined—these objects show elevated oxygen, sodium, and s-process element abundances. A similar pattern with respect to C, N, and the s-process elements has been reported in mildly metal-poor post-AGB stars (Reddy et al. 2002; van Winckel & Reyniers 2000). However, since these stars are only moderately metal poor, it is conceivable that this nitrogen abundance is of secondary origin and a result

of the first dredge-up (DUP). This possibility can be excluded for nitrogen in most C-rich EMP stars, where the N-abundance is much larger than the sum of the initially present C, N, and O abundances. In those cases where the binarity of a C-rich EMP star is established, the abundance of nitrogen and other elements may very well be the result of mass transfer from an AGB companion that now has evolved into a white dwarf.

IMSs may contribute to the abundance anomalies in globular cluster stars in the self-pollution scenario (Cottrell & Da Costa 1981; Denissenkov, Weiss, & Wagenhuber 1997). In particular, the observation of abundance anticorrelations in turnoff main-sequence stars (Gratton et al. 2001) has made it necessary to consider an external source for the abundance anomalies. Ventura, D'Antona, & Mazzitelli (2002) have proposed that the oxygen-sodium anticorrelation is due to the pollution of globular cluster members with material blown off TP-AGB stars. However, they have not explicitly included the Ne-Na and the Mg-Al H-burning cycle in their calculations of TP-AGB stars with $Z \geq 0.0004$. These reactions have been taken into account by Denissenkov & Herwig (2003), whose short study is partly based on models presented here in more detail. Finally, it should be noted that the TP-AGB phase of IMSs is the dominant source of dust in early galaxies of redshifts up to 5 (Morgan & Edmunds 2003).

IMSs during their TP-AGB evolution change their surface composition by two processes, the third DUP and envelope burning between TPs (which is also known as hot bottom burning, HBB). Low-mass stellar models of Population I metallicity with a combination of convective overshooting and high spatial and time resolution can reproduce the formation of low-luminosity carbon stars needed to explain the carbon-star luminosity function in the Magellanic Clouds (Herwig et al. 1997; Herwig 2000; Mowlavi 1999). Other consistency checks concerning the efficiency of overshooting at the various boundaries involve the effects of s-process nucleosynthesis (Lugaro et al. 2003; Herwig, Langer, & Lugaro 2003). The picture that has emerged from these studies of low-mass AGB stars that do not experience HBB is summarized in § 2. In § 3 the stellar evolution code and the model set are described. The results are presented in § 4, and conclusions are given in § 5.

2. TREATMENT OF CONVECTIVE BOUNDARIES

Hydrodynamic time- and depth-dependent overshooting may be present at all convective boundaries. An extended discussion of the motivation and background, as well as the technique of the exponential overshoot implementation used in this study, can be found in Herwig (2000) and Herwig et al. (2003). The overshooting efficiency in the deep interior cannot be determined from hydrodynamic models ab initio because of the large range of scales involved. In order to construct AGB models with some predictive power, one is therefore forced to constrain the overshooting efficiency semiempirically. At the bottom of the envelope of TP-AGB stars, exponential overshooting increases the DUP depth at almost any nonzero efficiency. With an efficiency $f \approx 0.15$, the resultant ^{13}C pocket that forms during the final period of the third DUP is massive enough to reproduce the observed s-process overabundances (Goriely & Mowlavi 2000; Lugaro et al. 2003; Herwig et al. 2003). Models with overshooting at the bottom of the PDCZ predict even more efficient third DUP, as well as a larger carbon and oxygen abundance in the intershell zone, compared with models that do not include overshooting at this convective boundary. The larger carbon abundance and, in

particular, the larger oxygen abundance in the intershell are in good agreement with the abundances observed in H-deficient central stars of planetary nebulae (of spectral type PG 1159 and [WC]-CSPN;[1] Koesterke & Hamann 1997; Dreizler et al. 1996) in conjunction with the latest models of the evolutionary origin of these stars (Herwig et al. 1999; Herwig 2001). These models predict that the PG 1159 and [WC]-CSPN stars show on their surfaces the abundance distribution of the intershell layer of the progenitor AGB star. In this context it is interesting to note that recent *FUSE* spectroscopic observations have established a significant Fe deficiency in some hot H-deficient central stars (Miksa et al. 2002). Further observations may substantiate the hypothesis that this Fe depletion is a result of the s-process in the intershell during the progenitor AGB evolution. This would support the claim that hot H-deficient central stars of planetary nebulae display directly the intershell material of their AGB progenitors.

However, in the s-process models, the larger carbon intershell abundance in models with overshooting leads to a larger neutron exposure in the s-process layer during the interpulse phase (Lugaro et al. 2003). In these models the s-process abundance distribution is too top-heavy, or in other words, the [hs/ls] index is larger than observed. This could be compensated by some weak mixing of the s-process layer during the interpulse phase (e.g., as a result of slow rotation; Herwig et al. 2003).

Models with exponential overshooting at the bottom of the PDCZ predict larger temperatures in the second s-process production location, fueled by the ^{22}Ne neutron source. Some branchings like the ^{96}Zr/^{94}Zr ratio are sensitively dependent on the temperature at the bottom of the PDCZ. At the same time, such isotopic ratios are experimentally known to high precision from mainstream presolar SiC grains, stemming from low-mass AGB stars (Zinner 1998; Nicolussi et al. 1998). This puts perhaps the most stringent constraint on the maximum possible overshooting efficiency. Although a more detailed study in this respect is still pending, preliminary calculations by Lugaro et al. (2003) indicate that low-mass models with $f_{\mathrm{PDCZ}} = 0.008$ may be in agreement with the temperature-dependent branchings and at the same time retain the enhanced oxygen intershell abundance indicated by the PG 1159 and [WC]-CSPN stars.

3. STELLAR EVOLUTION CODE AND MODEL CALCULATIONS

The models in this study were computed with the full one-dimensional stellar evolution code of Herwig (2000), including the exponential overshooting model described there. An earlier version of this code has been used by Blöcker (1995) to study the evolution of Population I AGB stars as a function of initial mass. As in most other AGB models, the Schwarzschild criterion for convection is used. The stabilizing effect of a μ-gradient as reflected by the Ledoux criterion is thus neglected. Using the Ledoux criterion in AGB stars would make it even more difficult to obtain the third DUP. In addition, the exponential overshooting included here would in this situation likely dominate mixing through semiconvection. In order to meet the high numerical resolution requirements of third DUP models, the adaptive time step and grid size routine was improved. It can now deal with the hot DUP burning episodes described below. In particular, it is ensured that the time step

---

[1] Central stars of planetary nebulae with Wolf-Rayet type spectrum.

and the grid resolution correspond to each other in the region near the bottom of the convective envelope during the DUP phase. In this situation, the Lagrangian advance rate of the bottom of the convective envelope $\dot{m}_{CE}$ implies a relation between the grid resolution and the time step. Numerical experiments indicate an appropriate Lagrangian scale in the third DUP overshooting zone to be $l_m = 10^{-6} \, M_{\odot}$, which should be well sampled in space and time. This means that the typical grid spacing in the DUP zone is less than $10^{-7} \, M_{\odot}$ and that the time steps should not be larger than $l_m / \dot{m}_{CE}$. In practice, this means that a single third DUP episode of several $10^{-3} \, M_{\odot}$ requires computing several thousand models. In the case where nuclear burning takes place during the DUP phase—as described below—the time step is further limited by the fluctuations of the hydrogen-burning luminosity L_H.

The opacities are from Iglesias & Rogers (1996; OPAL), supplemented with low-temperature opacities by Alexander & Ferguson (1994). The mixing-length parameter has been set to $\alpha_{MLT} = 1.7$, as calibrated by fitting a solar model. The nuclear network equations and the time-dependent mixing equations are solved simultaneously, using a fully implicit, iterative scheme. For this study an automatic sub–time step algorithm has been implemented into the Newton-Raphson scheme. If the convergence criteria are not met within five to eight iterations, the time step is replaced by a 10 times smaller sub–time step, followed by a second sub–time step that takes care of the remaining 90% of the original time step. This procedure can be applied repeatedly and guarantees that a solution with the predefined precision can be found even in fairly violent burning and mixing events, as encountered in massive AGB models of very low metallicity. All relevant charged particle reactions are included, up to and including the Mg-Al cycle, as well as neutron captures. Reaction rates are mainly based on Caughlan & Fowler (1988). Updates from El Eid & Champagne (1995) and from Angulo et al. (1999) for the important CN-cycle p-capture rates have been considered.

The benchmark model sequence (E79-D4; see Table 1) has an initial mass of $5 \, M_{\odot}$ and a metallicity of $Z = 0.0001$ ([Fe/H] $\approx \log (Z/Z_{\odot}) = -2.3$). It is evolved from the pre–main sequence through all evolutionary phases up to the AGB. For the initial helium mass-fraction abundance, we adopt $Y = 0.23025$ according to

$$Y = Y_{\odot} + \frac{\Delta Y}{\Delta Z} (Z - Z_{\odot}),$$

where $Y_{\odot} = 0.28$ is the value adopted for the solar initial helium abundance (Grevesse & Noels 1993; Grevesse & Sauval 1998), and $Z_{\odot} = 0.02$ has been adopted for the solar metallicity. $\Delta Y / \Delta Z$ is the ratio of fresh helium to metals supplied to the interstellar medium by stars. The value of 2.5 used in this study is consistent with many observational constraints (e.g., Pagel & Portinari 1998 and references therein).

Many stars of low metallicity may, in fact, form from gas clouds that have a nonsolar abundance distribution. For example, Carney (1996) concluded in his review of observational data that globular cluster stars with [Fe/H] ~ -0.6 are overabundant in the α-elements by a factor of about 2. However, some halo stars have been reported with solar-scaled α-element abundances (Nissen & Schuster 1997). For this study we have adopted a solar-scaled metal distribution according to Grevesse & Noels (1993) and Anders & Grevesse (1989). Most of the results discussed here are related to the production and processing of primary C and O, which dominate the surface abundance evolution once DUP starts.

Mass loss has not been considered for the $5 \, M_{\odot}$ cases, on which most of this investigation is based. This choice was motivated by the fact that model tracks with mass loss show less DUP (Karakas et al. 2002). Besides, the amount of mass loss that occurs in very low metallicity stars is uncertain. Because of the lack of mass loss, the calculations do not have a natural end due to the loss of the stellar envelope. At least one sequence is followed through 15 TPs, which is sufficient to reach the asymptotic regime in which changes of many quantities are smaller and more regular than during the initial TP-AGB phase.

Up to the first TP on the AGB, exponential overshooting with $f = 0.016$ is applied at all convective boundaries. This is the same value as used by Herwig (2000), and it was originally obtained by calibrating core overshooting to reproduce the observed width of the main sequence. For the TP-AGB benchmark case (sequence E79-D4), a nonzero but negligible overshooting efficiency[2] of $f_{PDCZ} = 0.002$ at the bottom of the PDCZ and the previously used value of $f_{CE} = 0.016$ at the bottom of the convective envelope are applied at all times—during the HBB interpulse phase as well as during the DUP phase. In our opinion, this choice represents a minimum overshooting situation. AGB models with such overshooting parameters would not generate enough ^{13}C for the s-process production during the intershell, and they would not be able to reproduce the observed abundances of PG 1159 stars and [WC]-CSPN (§ 2). For this reason, the possibility of larger overshooting efficiency is explored by a number of test computations (Table 1, § 4.5). Rotation and the possible effects of magnetic fields are not included.

4. RESULTS

4.1. Pre-AGB Evolution

The $5 \, M_{\odot}$ pre–main-sequence model is evolved through all phases up to the giant stage. The evolution track is in good agreement with calculations by Girardi et al. (1996; see our Fig. 1). The small remaining differences can be attributed to differences in overshooting efficiency, mixing-length parameter, and other details of the physical inputs and numerical techniques. The core H- and He-burning times—in particular, the sum of both—are in reasonable agreement as well. This model has $\tau_H = 8.64 \times 10^7$ yr and $\tau_{He} = 1.21 \times 10^7$ yr, compared with $\tau_H = 9.00 \times 10^7$ yr and $\tau_{He} = 9.13 \times 10^6$ yr

TABLE 1
Model Sequences Used in This Paper

Track ID	f_{PDCZ}	f_{CE}	$M_{ZAMS}/M_{\odot}$	Z
E79-D4[a]	0.002	0.016	5	0.0001
E79-D9	0.016	0.016	5	0.0001
E79-D10/D11	0.002	≥0.032	5	0.0001
E37-D2	0.016	0.016	5	0.02
E85-D2	0.016	0.008	4	0.0001

[a] Benchmark sequence.

[2] This small amount of overshooting has very little effect on the He-flash peak luminosities and intershell abundances, but behaves numerically more benign with the simultaneous solution of time-dependent mixing and nuclear burning.
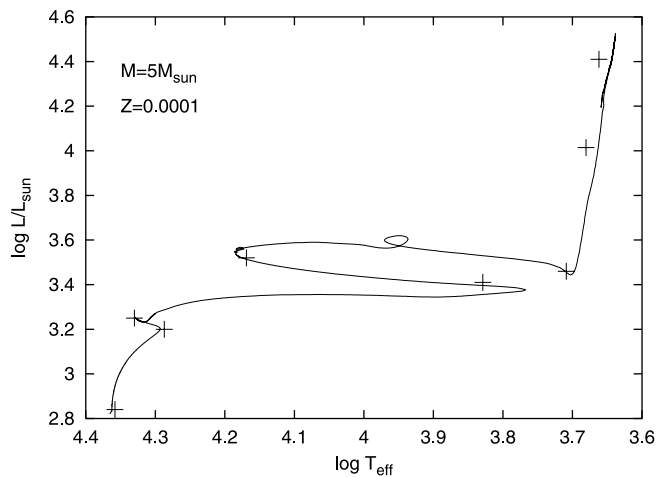
FIG. 1.—H-R diagram of pre-AGB evolution. The plus signs along the track indicate selected points along an evolution sequence computed by Girardi et al. (1996) with the same initial mass and metallicity.

for the model by Girardi et al. (1996). Initially, the mass of the main-sequence core convection zone is 1.33 $M_\odot$, and it decreases to $\sim$0.45 $M_\odot$ shortly before H burning in the core ceases. The maximum extent of the convective He-burning core is 0.55 $M_\odot$, and one major breathing pulse has been found. At the end of the core He-burning phase, the H shell is located at $m_r = 1.47$ $M_\odot$. The second DUP starts 4.25×10^6 yr after the end of the He-core burning when the bottom of the convective envelope reaches into the H-free core. This mixing episode ends after 63,000 yr when the bottom of the envelope has reached $m_r = 0.9615$ $M_\odot$.

IMSs at this low metallicity do not have a first giant branch phase (Girardi et al. 1996), and thus the first envelope abundance alteration occurs as a result of the second DUP. Material processed mainly by H-shell burning is brought to the surface. ^{4}He is enriched by about 50% to $X(^4\mathrm{He}) = 0.335$, and hydrogen is reduced accordingly to $X(\mathrm{H}) = 0.65$. Compared with the very efficient production of ^{14}N by the combined action of HBB and the third DUP later during the TP-AGB evolution, the second DUP of ^{14}N with an enhancement by
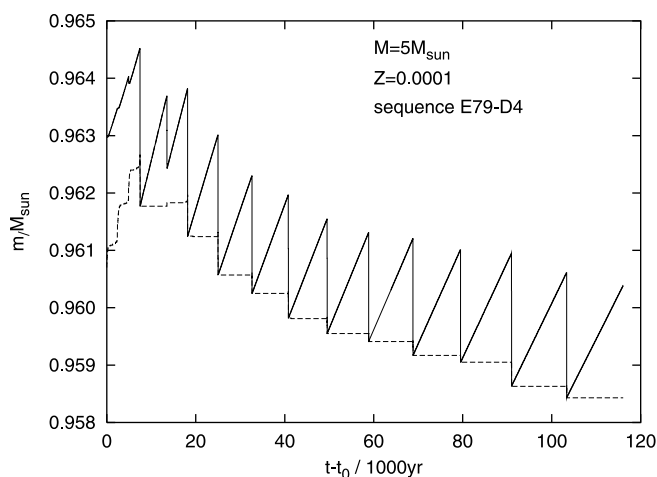
$\sim$50% can be considered unimportant. ^{23}Na is enhanced by 0.75 dex from the conversion of the initial abundance of ^{22}Ne and some ^{20}Ne (see also § 4.4.3). ^{16}O is depleted by 0.1 dex because of partial ON cycling. Magnesium isotopes are changed by less than 0.05, 0.1, and 0.01 dex for mass numbers 24, 25, and 26 in the second DUP. The first He-shell flash occurs 12,200 yr after the end of the second DUP. At this time the H-free core has a mass of 0.9630 $M_\odot$.

4.2. Envelope Burning and Third Dredge-up

The entire chemical enrichment is strongly dependent on the occurrence of the third DUP. The 5 $M_\odot$ TP-AGB model sequence shows efficient third DUP after the fourth TP (Fig. 2). The DUP mass is almost $\Delta M_{\mathrm{DUP}} = 3 \times 10^{-3}$ $M_\odot$, comparable to the DUP in a low-mass AGB star with $\lambda = 0.5$. This DUP parameter is defined as $\lambda = \Delta M_{\mathrm{H}}/\Delta M_{\mathrm{DUP}}$, where ΔM_{H} is the core mass growth due to H burning during the interpulse phase. All following TPs have a very efficient third DUP as well. The fifth TP is an exception because the time step control algorithm failed. As a result, the DUP efficiency is too small (Fig. 2). For all subsequent TPs the DUP parameter always exceeds unity, and the H-free core M_{H} effectively shrinks slightly. This is also true for the He-free core M_{He}. The evolution of the He- and H-burning luminosity, as well as the stellar radius and the stellar luminosity, of the 5 $M_\odot$ model is shown in Figures 3 and 4. Note how the surface properties, as well as the evolution of the shells, change at the onset of deep DUP. The evolution of shell luminosities and surface parameters differs strongly from the situation in more metal-rich and/or less massive models (Lattanzio 1992; Blöcker 1995; Herwig 2000).

A more detailed presentation of the sixth TP is given in Figure 5. The evolution of the bottom of the envelope convection zone is very smooth. In various test sequences the time evolution of this convective boundary showed discontinuous steplike advances into the core. In these tests the numerical resolution was insufficient. Such features cannot be

FIG. 2.—Evolution of the hydrogen-free core [solid line; defined as $M_{\mathrm{H}} = m_r(X_{\mathrm{H}} < 0.37)$] and the helium-free core (dashed line; defined as $M_{\mathrm{He}} = m_r(X_{\mathrm{He}} < 0.49)$] during the TP-AGB; $t_0 = 99{,}385{,}139.9$ yr at maximum of L_{He} during the first TP ($M = 5$ $M_\odot$, $Z = 0.0001$, sequence E79-D4). See text for an explanation of the small DUP at $t - t_0 \sim 15 \times 10^3$ yr.
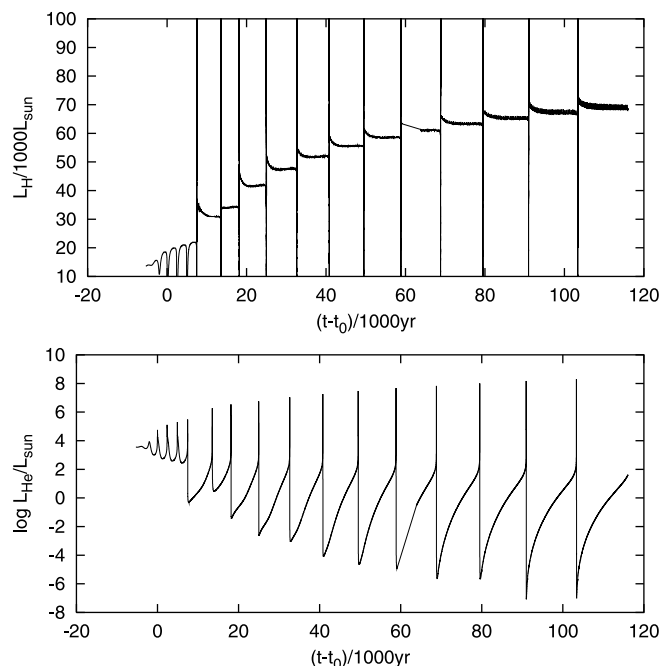

FIG. 3.—Evolution of the hydrogen-burning luminosity (top) and the helium-burning luminosity (bottom) for the same sequence as shown in Fig. 2.
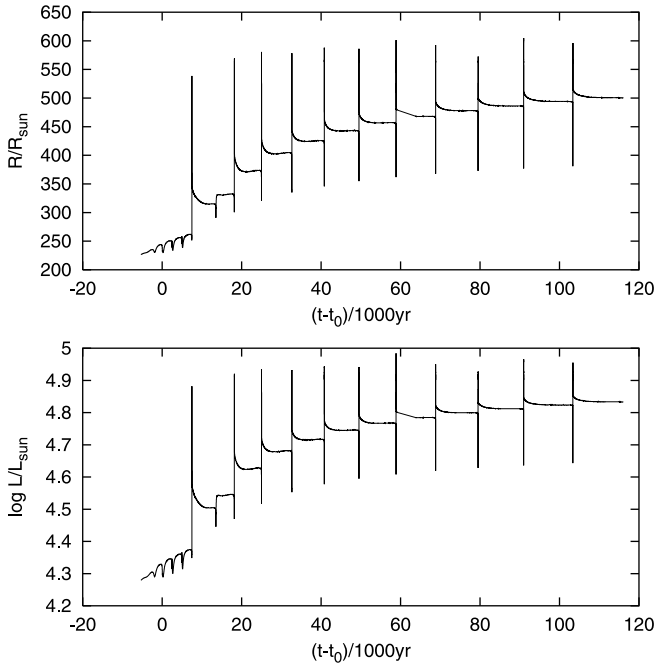
Fig. 4.—Evolution of the stellar radius (*top*) and the stellar luminosity (*bottom*) for the same sequence as shown in Fig. 2.

found during the DUP after the sixth or any subsequent TP of the benchmark 5 $M_\odot$ sequence. In this model sequence, the third DUP, in particular, with respect to the Lagrange location of the He-burning shell ($M_{\rm He}$) and the PDCZ, is very deep. The envelope convection not only engulfs the entire interpulse zone, but it even penetrates into the He-free core. This third DUP behavior is not present in more metal-rich massive AGB models or in low-mass AGB models. A decreasing $M_{\rm He}$ has previously been reported by Herwig (2000, Table 1) for the TP-AGB evolution of a $M_{\rm ini} = 4\ M_\odot$ sequence with $Z = 0.02$. However, for that sequence, efficient overshooting ($f_{\rm PDCZ} = 0.016$) at the bottom of the PDCZ has been assumed, which leads to a deep penetration of the PDCZ into the C/O core beneath the He shell. This is not the case in the present model, which has been computed with negligible overshooting at the He-shell flash boundary ($f_{\rm PDCZ} = 0.002$). The
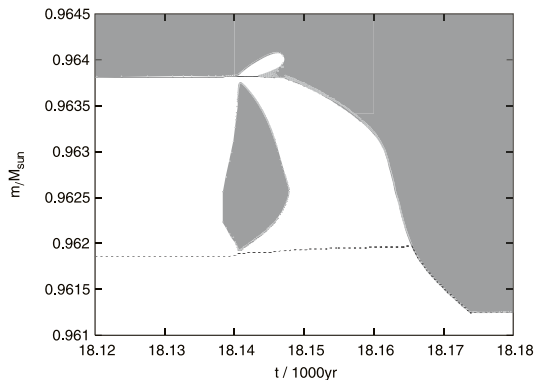

Fig. 5.—Evolution of the hydrogen-free core, the helium-free core, and the convection zones during the sixth TP ($M = 5\ M_\odot$, $Z = 0.0001$, sequence E79-D4). Except for a short period immediately after the He flash at $t = 18.14 \times 10^3$ yr, the bottom of the envelope convection zone and the H-free core coincide in this representation. Note that the third DUP penetrates into the He-free core; $t_0 = 99{,}385{,}139.9$ yr at maximum of $L_{\rm He}$ during the first TP.

bottom of the PDCZ does not penetrate significantly into the He shell, and consequently the intershell abundances are not enhanced with carbon and oxygen, as has been found in models with efficient PDCZ overshooting. The mass fractions in the PDCZ of the sixth TP are $(^4{\rm He}/^{12}{\rm C}/^{16}{\rm O}) = (0.854/0.143/0.002)$ (see below for the tenth TP).

In all successive TPs, deep DUP reaching below the He shell is present, although the mass dredged up from below the He shell decreases somewhat (Fig. 2). The events during the tenth TP are shown in detail in Figure 6. The four abundance profile panels (i–iv) show the situation at the successive times indicated in the top panel. Panel (i) shows the situation shortly before the onset of the He-shell flash. The dip in the ^{16}O profile at location A is a signature of the H shell. In the convective envelope (*light shaded region*), ^{14}N is the most abundant species of the CNO elements, indicating efficient HBB. At location B, the large abundance of ^{14}N reveals the nature of this material as H-shell ashes. Toward location C, ^{12}C and ^{16}O, and as well ^{22}Ne, gradually increase in abundance, while ^{14}N decreases as a result of α-capture reactions. Location C harbors He-shell ashes that constitute the top layer of the C/O core.

Shortly after $t = 49.51 \times 10^3$ yr, the He-shell flash drives the PDCZ. Panel (ii) of Figure 6 shows the abundances at the peak extension of the PDCZ (*darker shading*). Just above $m_r = 0.9615\ M_\odot$, the tiny He buffer and the signatures of the H shell can be seen. Thus, the PDCZ does not reach into the H-rich envelope and no protons are ingested into the convection zone. Such an occurrence has been suggested to be an alternative site for the s-process in EMP or zero-metallicity TP-AGB stars (Aoki et al. 2001). If such a mixing event occurs in IMSs, it should be restricted to metallicities lower than the one studied here ($Z = 0.0001$).

During the pulse, ^{14}N is synthesized into ^{22}Ne and, to some extent, into ^{25}Mg. The latter is the result of the $^{22}{\rm Ne}(\alpha, n)^{25}$Mg reaction, which releases neutrons for the s-process. In addition, ^{12}C and ^{16}O are now present in the intershell with a larger abundance than before the He flash [$(^4{\rm He}/^{12}{\rm C}/^{16}{\rm O}) = (0.782/0.198/0.017)$]. The ^{16}O abundance now exceeds 1% by mass, a value that is very similar to predictions of more metal-rich models obtained without overshooting (Schönberner 1979). We discuss in § 4.5 how the abundance of this primary oxygen depends on the overshooting. However, the presence of 1%–2% of oxygen by mass in the intershell of AGB stars after a few initial TPs should be considered as a *minimum* at *any* metallicity. The third DUP will mix this primary oxygen into the envelope. In stars of solar or only mildly subsolar metallicity, the presence of primary oxygen might be unnoticeable observationally, partly because of the inherent difficulties in determining oxygen abundances and partly because the initial oxygen abundance is very close or even equal to the oxygen abundance in the intershell. However, this obviously changes in TP-AGB stars of very low metallicity. If the initial envelope abundance has an extremely low CNO abundance, then the DUP of material containing $X(^{16}{\rm O}) = 0.02$ should be noticeable. In fact, the zero-metallicity models of both Chieffi et al. (2001) and Siess et al. (2002) report a significant fraction of oxygen in the dredged-up material that is especially obvious in the less massive cases without very efficient HBB. From the intershell abundances reported here, one can immediately make some simple predictions. For example, if a hypothetical EMP star has a C overabundance of [C/Fe] = 2.5, and if this C abundance comes from the heavy pollution by a TP-AGB star that has not experienced very efficient
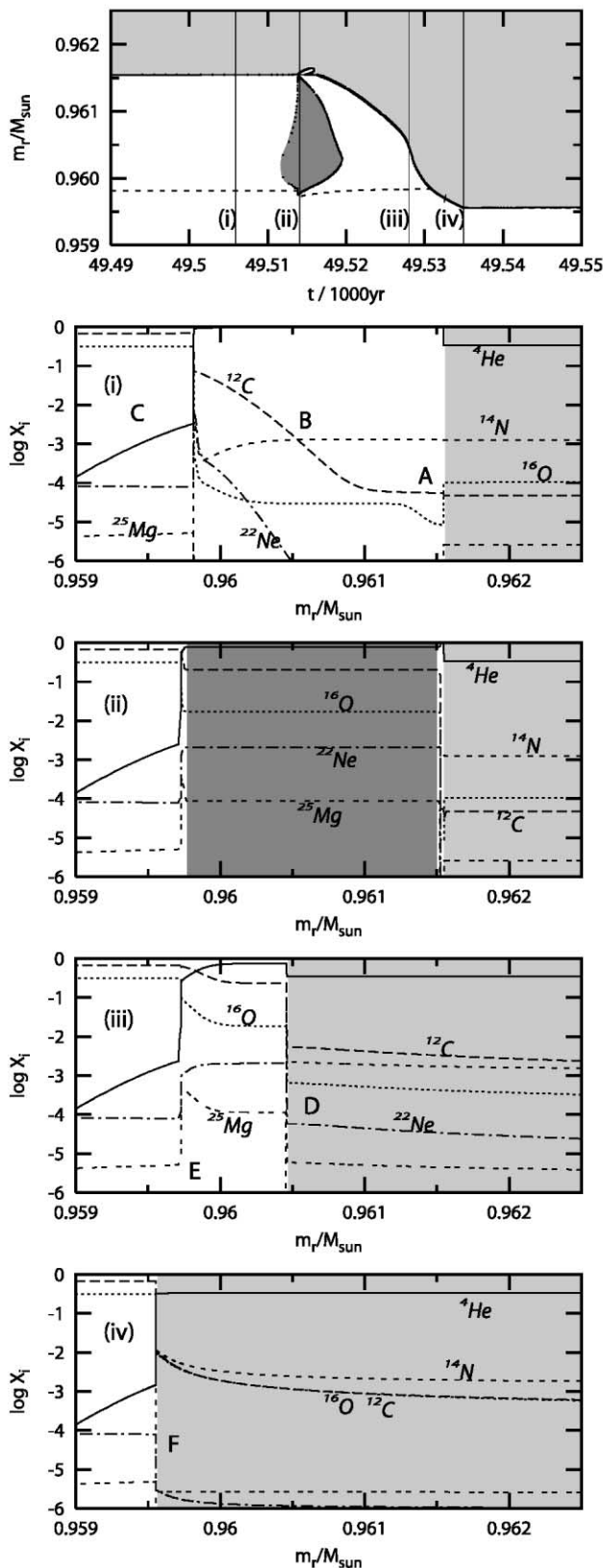
FIG. 6.—*Top*: Evolution of the Lagrangian location of the H- and He-burning shells and the convectively unstable layers (*dark shade*, PDCZ; *light shade*, envelope convection). (i–iv) Abundance profiles at times indicated by thin vertical lines in top panel. Labeled regions of special interest are discussed in the text. A blow-up of region F in panel (iv) is shown in Fig. 8. [*See the electronic edition of the Journal for a color version of this figure.*]

HBB (which would have destroyed some O), then the prediction for oxygen would be $[O/Fe] \gtrsim 1.5$. This is so simply because the predicted X_C/X_O ratio in the dredged-up material is $\lesssim 10$.

In panel (iii) of Figure 6, the situation during the third DUP following the He flash is shown. In location D the bottom of the envelope proceeds inward, bringing to the surface ^{12}C, ^{16}O, ^{22}Ne, and other species. This ^{22}Ne is the seed for ^{23}Na production by HBB. In location E of panel (iii), a small ^{25}Mg pocket has formed from the α-capture reaction on ^{22}Ne, which releases neutrons for the *s*-process. The neutrons released during the production of this ^{25}Mg pocket are in addition to the neutrons from the ^{22}Ne neutron source considered in the present *s*-process models. These neutrons are released during a high-T radiative ^{22}Ne burning phase (along the dashed line in the top panel of Fig. 6) between $t = 49.515 \times 10^{-3}$ yr and $t = 49.53 \times 10^{-3}$ yr. The temperature during this 15 yr period of time decreases from the peak PDCZ value of $\log T = 8.55$ to $\log T = 8.3$, and for 10 out of the 15 years, $\log T > 8.4$. In more metal-rich or lower mass TP-AGB models, the DUP never reaches this layer. Consequently, present *s*-process models do not need to consider these neutrons, which usually are buried in the core. However, in this massive TP-AGB model of very low metallicity, the DUP picks this material up as it reaches below the He shell. This is shown in panel (iv), where the situation at the end of the third DUP is shown.

Two interesting things can be seen in panel (iv). First, because the DUP now reaches below the He shell, additional primary oxygen is brought to the envelope in significant amounts. Thus, oxygen is dredged-up efficiently, despite the fact that practically very inefficient overshooting has been assumed at the bottom of the PDCZ. Second, the ^{14}N abundance in the bottom region of the convective envelope exceeds the C and O abundance. This means that H burning already takes place at the bottom of the envelope. HBB has already started and processes C and O dredged-up from the core in situ.

This DUP is *hot*, as opposed to the situation in less massive or more metal-rich TP-AGB stars. In sequence E79-D4, the peak H luminosity during the efficient hot DUP events is in the range $(1.4 - 1.8) \times 10^6 L_\odot$ and is not changing in a systematic way from pulse to pulse. The large H luminosity leads to a peak in the surface luminosity (Fig. 4). At low metallicity the envelope reaches faster into deeper and hotter layers than at higher metallicity. The temperature in the overshooting layer during the DUP remains below the value obtained in the H shell during subsequent HBB. However, the ^{12}C abundance is much higher in the intershell then in the H shell. Therefore, H burning is not limited by the slow *p*-capture of ^{14}N, but only by the faster ^{12}C$(p,\gamma)^{13}$N reaction. In Figure 7 the energy generation, temperature, and H and ^{12}C profiles across the convective boundary are shown. The nuclear energy production by H burning in the overshooting layer during DUP is several orders of magnitude greater than in the H shell during HBB and, in particular, is vigorous in the exponential overshooting zone. However, even within the convective envelope the H-burning luminosity is still significant. In this innermost region of the convective envelope, the abundances of ^{12}C and ^{14}N are determined by both mixing and *p*-capture nucleosynthesis. Because of the coupled treatment of time-dependent mixing and nucleosynthesis, the models predict a continuous decrease from the large intershell values to the small envelope abundance. In the transition zone at the very bottom of the envelope convection, the H-burning luminosity decreases gradually outward from the peak value in the overshooting
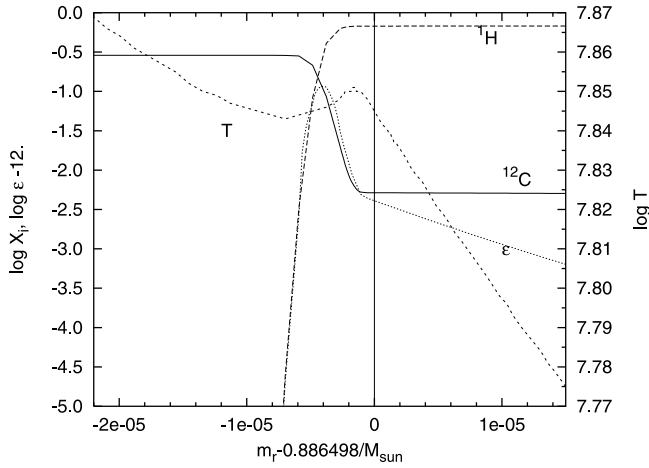
FIG. 7.—Profiles of protons, ^{12}C, nuclear energy generation ϵ (*left scale*), and temperature (*right scale*) at the bottom of the convective envelope during the DUP of sequence E85 ($Z = 0.0001$). The abscissa has been shifted by the mass coordinate of the envelope convection boundary, and the region to the right of the vertical line is the convective envelope.

layer. For large core masses, as for the benchmark 5 $M_\odot$ case E79, this additional luminosity increases the DUP efficiency. Since the radiative temperature gradient is proportional to the luminosity ($\nabla_{\rm rad} \sim l$), efficient H burning during the DUP increases the convective instability, and models including this effect show more efficient envelope enrichment at each TP. In § 4.5 the dependence of this effect on the overshoot parameter is discussed.

The H burning during the DUP has been noted before for $Z = 0$ TP-AGB models with a small amount of overshooting by Chieffi et al. (2001). Their H-burning luminosities are even similar. However, only one or two pulses with this hot DUP have been followed because of the numerically demanding nature of this phase.

In addition to the $Z = 0.0001$ models, a comparison sequence with $Z = 10^{-5}$ has been computed. Overall, the properties are very similar. In particular, the deep DUP, the hydrogen burning during the DUP phase, and the efficient ^{14}N production through HBB is found in the IMSs of the lowest metallicities. In the EMP cases, the envelope CNO abundance is dominated by the primary component from the third DUP. It is this envelope CNO abundance that determines to a large extent the evolution of envelope-burning AGB stars, including their yields. Since DUP is so efficient and sets in very early, stars with even lower metallicity than $Z = 0.0001$ still behave in a very similar way.

4.3. s-Process Considerations

The main nuclear production site of the *s*-process elements is usually associated with low-mass TP-AGB stars (Gallino et al. 1998; Busso, Gallino, & Wasserburg 1999; Goriely & Mowlavi 2000; Busso et al. 2001; Lugaro et al. 2003; Herwig et al. 2003). This, however, does not imply that massive AGB stars do not synthesize the *s*-process elements at all. Very little is known theoretically about the *s*-process at very low metallicity. IMSs of this metallicity may have a distinctive *s*-process signature that can be used as a diagnostic tool for the interpretation of observations. Two reactions can release significant amounts of neutrons in conditions encountered in TP-AGB stars. The ^{13}C$(\alpha, n)^{16}$O reaction is efficient for $\log T > 7.95$, while the ^{22}Ne$(\alpha, n)^{25}$Mg reactions require $\log T > 8.45$ to release significant amounts of neutrons.

According to current models of the *s*-process in low-mass stars, ^{13}C releases neutrons under radiative conditions during the interpulse phase and provides most of the neutrons in the majority of enriched stars. It is also believed that this neutron source is responsible for *s*-process isotopic signatures found in presolar meteoritic SiC grains. For this mechanism, protons have to be partially mixed with ^{12}C at the intershell-envelope interface at or immediately after the end of the third DUP. This partial-mixing zone will heat up as the intershell layer contracts to the preflash configuration. Then ^{13}C forms, which at a later phase during the interpulse will capture α-particles and release neutrons. This scenario has been very successfully applied in conjunction with stellar evolution models that do assume an ad hoc H profile for the partial-mixing zone. As discussed in § 2, recent studies of the effects of rotation and/or overshooting as a physical mechanism for the required mixing have revealed a more complicated picture that is not yet well understood.

In the very low metallicity IMSs with deep DUP, a partial-mixing zone forms at the end of the third DUP as a result of the overshooting algorithm. The first difference compared with the low-mass models is that the ^{13}C pocket forms immediately. As shown already in the previous section, the temperature at the bottom of the convective envelope is high enough for H burning during the actual DUP period. The narrow ^{13}C pocket at the end of the third DUP episode of the tenth TP (corresponding to panel [iv] in Fig. 6) is shown in Figure 8. The ^{14}N pocket, which acts as a neutron poison, is also evident. Since the DUP has reached below the He shell, the mole fraction of ^{4}He [for the subsequent activation of the ^{13}C$(\alpha, n)^{16}$O reaction] is only a fraction of the ^{13}C abundance in the pocket. For this reason, the ^{13}C neutron source may be not or only inefficiently available in these massive TP-AGB models.

The (α, n) reaction of ^{22}Ne releases neutrons in the He shell during the He flash. This neutron source is activated very efficiently. ^{14}N, from which ^{22}Ne is generated, is the result of CNO cycling on previously dredged-up primary C and O. The neutron source efficiency therefore depends on the peak temperature that is reached, as well as on the cumulative efficiency of previous DUP episodes. In this model the third DUP is
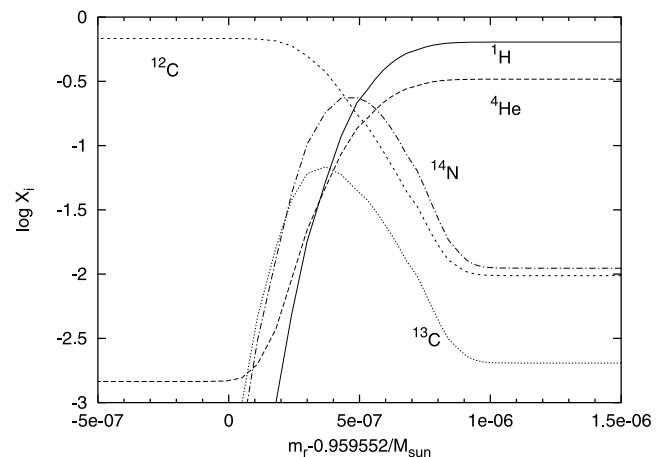

FIG. 8.—Abundance profiles of species relevant for the *s*-process in region F of Fig. 6 (panel iv). The region on the left is the top layer of the C/O core; the region on the right is the bottom of the envelope convection zone at the end of the third DUP after the tenth TP. The helium abundance in the layer below the convection zone is low because the third DUP has reached below the He shell (see text).

very efficient and therefore the ^{14}N abundance in the ashes of the He shell is rather large. This enhances the neutron release in the PDCZ, and this effect is obviously more pronounced at lower metallicity. A second contribution comes from radiative ^{22}Ne burning already mentioned in § 4.2. Following the peak of the He-shell flash, the temperature in the He shell gradually decreases. At this time the actual He shell is no longer convectively unstable. Neutron captures may still be possible, but now under radiative conditions. Later this layer will be picked up by the third DUP. This second contribution will likely not exceed 10% of the s-process synthesis in the PDCZ but may be important for details at certain branchings. Finally, it may be worth considering the effect of ^{13}C left behind in the H-shell ashes. Since the primary CNO abundance can be quite large because of efficient DUP, the ratio of ^{13}C to ^{56}Fe seed will be much more favorable than in more metal-rich stars. On the other hand, because of the large ^{14}N/^{13}C ratio in the H-shell ashes, the efficiency of the trans-iron element production will be limited. A quantitative analysis of the s-process in these models will be presented elsewhere.

4.4. Surface Abundance Evolution

4.4.1. H and He

During the TP-AGB phase the envelope abundance is altered by the combined effect of DUP and envelope burning. After 14 TPs the envelope hydrogen abundance of the E79-D4 sequence has decreased from initially $X(\mathrm{H}) = 0.665$ to 0.654. Initially, the H abundance changes mainly because of the third DUP. However, after the eighth TP, the H destruction due to HBB dominates, and during the following TPs the H depletion follows a roughly linear decrease with time that can be approximated by

$$X(\mathrm{H}) = -1.3 \times 10^{-4} t_3 + 0.6669,$$

with $t_3 = t/1000$. Correspondingly, the ^{4}He abundance increases from $X(^4\mathrm{He}) = 0.335$ to 0.343 and follows approximately the relation

$$X(^4\mathrm{He}) = 1.15 \times 10^{-4} t_3 + 0.3327.$$

4.4.2. C, O, and Primary N

The combined CNO abundance increases steadily and follows the relation

$$X(\mathrm{C} + \mathrm{N} + \mathrm{O}) = 2.1 \times 10^{-5} t_3 + 4.0 \times 10^4.$$

Thus, at each TP, the mass fraction of CNO material in the envelope increases by $\Delta X \approx 2 \times 10^{-4}$. The relative abundance of the CNO isotopes changes periodically with the pulse phase (Fig. 9). After the onset of efficient third DUP, the temperature during the interpulse phase at the bottom of the convective envelope (HBB temperature) quickly settles into the range $(9.1–9.6) \times 10^7$ K. Primary C and O dredged up from the intershell is cycled into ^{14}N. Part of that cycling occurs immediately during the DUP, which can be seen from the increase of ^{13}C together with ^{12}C and ^{16}O at the DUP time (§ 4.2). During this short H-burning DUP phase, the ^{12}C/^{13}C ratio rises to values in the range 6–7, which is much larger than the CNO cycle equilibrium value of ∼3.5 that is obtained in the envelope in the second half of the interpulse cycle because of HBB.
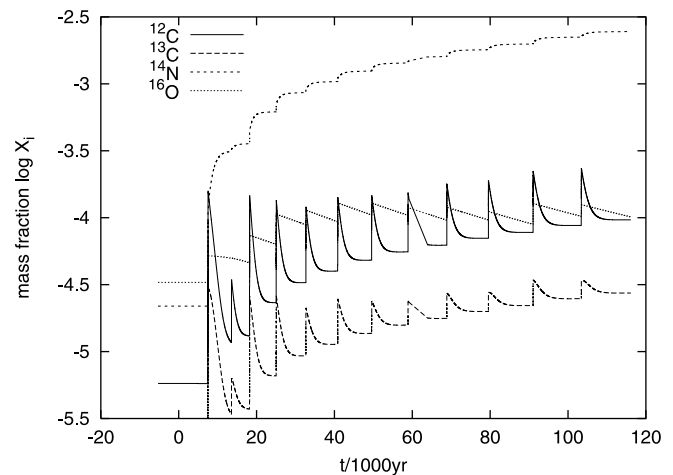

Fig. 9.—Envelope abundance evolution of relevant CNO isotopes for the 5 $M_\odot$ benchmark case (E79-D4). Two irregular behaviors can be seen. At $t \sim 15 \times 10^3$ yr, the DUP is smaller than after the preceding and the following TP as the result of insufficient numerical resolution (see § 4.2 for details). At $t \sim 62 \times 10^3$ yr, some data files for the plot routine were lost, and the HBB phase following the TP—most notably of ^{12}C—is not plotted accurately.

Even though the HBB temperature is high enough to burn oxygen, the effect of oxygen DUP is clearly noticeable. In this model, third DUP of oxygen prevents an efficient ^{16}O depletion by HBB. The oxygen isotopic ratios evolve toward ^{16}O/^{17}O $\gtrsim 100$ during the interpulse phase, but larger values (120–180) are present in the envelope during the earlier TPs, and in particular during the H-burning DUP events. The ratio ^{16}O/^{18}O $\gtrsim 2 \times 10^6$ at all times.

The most important aspect of the CNO abundance evolution is the significant primary ^{14}N production. After the 14 TPs computed here without mass loss, the ^{14}N abundance is twice the solar ^{14}N abundance. The envelope, which will be lost eventually, of this model star contains at this point approximately 8×10^{-3} $M_\odot$ of primary ^{14}N.

4.4.3. Oxygen and Sodium

The elemental abundance evolution of sodium and oxygen is correlated or stationary in all models reported here. Oxygen in the envelope increases because of DUP and decreases because of HBB. In this model these two effects balance each other. Sodium forms early on in the pulse cycle and is then destroyed again. This concordance can easily be explained. ^{22}Ne—the seed for ^{23}Na—follows indirectly the DUP of primary C and O from the intershell, since it is made from the ^{14}N that results from H-shell burning of the dredged-up C and O material. If the envelope-burning temperature is large enough for the ^{22}Ne$(p, \gamma)^{23}$Na reaction, then the production of ^{16}O and ^{23}Na is correlated. The destruction, on the other hand, is also correlated because the p-capture rates of both isotopes are very similar (Angulo et al. 1999).

Denissenkov & Herwig (2003) have discussed the implications of these processes in massive AGB stars for the O-Na anticorrelation in globular clusters. They have argued that low-metallicity IMSs are probably not directly responsible for the observed O-Na anticorrelation. An important detail in their argument is the recurrent DUP of oxygen (§ 4.2), which would require larger HBB temperatures for effective oxygen depletion. At such large temperatures any sodium produced by p-capture on ^{22}Ne would be destroyed as well. In a star with lower HBB temperatures, simultaneous oxygen and sodium

enhancement is predicted. In any case, AGB stellar models predict an O-Na correlation, or no correlation, rather than an anticorrelation. In Figure 10 the sodium and oxygen abundances, the globular cluster stars, and the model prediction from this work are compared. The globular cluster stars show a varying degree of oxygen depletion that is associated with a sodium enhancement.

The offset in sodium abundance between the model abundances and the globular cluster stars can be fully attributed to the choice of initial composition for the models. The TP-AGB initial sodium abundance of the models, which corresponds to [Na/Fe] ~ 0.6 and [O/Fe] ~ -0.2 (Fig. 10), is the result of the second DUP, during which the envelope convection reaches into the ashes left behind by the H shell. In the H shell, primordial ^{22}Ne is partially transformed into ^{23}Na. The initial sodium abundance of the TP-AGB model corresponds to an initial solar-scaled ^{22}Ne abundance. While no observational information on the noble gas neon is available for low metallicities, theoretical models of Galactic chemical evolution agree that [Ne/Fe] is larger at lower [Fe/H]. At [Fe/H] $= -2.5$, the predictions range from [Ne/Fe] $= +0.2$ (Timmes, Woosley, & Weaver 1995) to [Ne/Fe] $= +0.7$ (Alibés, Labay, & Canal 2001). However, this is predominantly ^{20}Ne, since ^{22}Ne is a secondary isotope and follows the initial abundance of ^{14}N in massive stars (Woosley & Weaver 1995). Unless the parent cloud of the AGB stars modeled here has been polluted by an even earlier generation of massive AGB stars, its ^{22}Ne abundance has probably been negligible. In that case, the initial sodium abundance of the $Z = 0.0001$ massive TP-AGB stellar models is the same as the initial sodium abundance at the time of star formation. In order to explain the O-Na anticorrelation in globular clusters by simultaneous Na production and O destruction, it is often assumed that [Na/Fe] $\lesssim 0$ initially at low metallicity. This is in agreement with theoretical models of Galactic chemical evolution (Timmes et al. 1995; Alibés et al. 2001), although a systematically lower [Na/Fe] at lower [Fe/H] is not obvious

from the analysis of field giants by Gratton et al. (2000). However, they report a scatter of $\sim \pm 0.3$ around [Na/Fe] $= 0$ for $-2.5 <$ [Fe/H] < -0.5.

4.4.4. Magnesium

The magnesium isotopic ratios can be modified by three processes in AGB stars: (1) α-captures on ^{22}Ne in the He shell (flash), which can produce both ^{25}Mg and ^{26}Mg, (2) p-captures on ^{24}Mg and ^{25}Mg during the envelope-burning phase, and (3) n-captures on ^{24}Mg and ^{25}Mg, as well as on ^{26}Al. In Denissenkov & Herwig (2003) the TP-AGB evolution dominated by high HBB temperature is discussed, during which the initially available ^{24}Mg burns mainly into ^{25}Mg. In cases of lower HBB temperature (either because of the inclusion of mass loss or because of a smaller mass), and if a complete treatment of neutron capture reactions is taken into account, the other two effects operating in the PDCZ become more important for the model predictions.

4.5. Dependence on the Overshooting Parameter

Three additional tracks with different assumptions on the overshooting efficiency have been calculated (Table 1). Comparison of sequences D4 and D9 reveals the influence of the overshooting parameter at the bottom of the PDCZ. For sequence D9 a larger overshooting efficiency ($f_{\text{PDCZ}} = 0.016$) than for sequence D4 has been assumed. These tests confirm the trends found for the 3 $M_\odot$, $Z = 0.02$ stellar model with intershell overshooting by Herwig (2000). In comparison to the D4 sequence, the D9 sequence shows the following:

1. A Larger L_{He}-flash peak luminosity by roughly a factor of 1.5–2.

2. A longer interpulse period by $\sim 20\%$.

3. A slightly smaller DUP H-burning luminosity and similar quiescent interpulse H-shell luminosity.

4. A larger third DUP; e.g., at the sixth TP of the D9 sequence at $t - t_0 = 35,384$ yr (t_0 as in Fig. 2), the DUP parameter is $\lambda = 1.46$, compared with $\lambda = 1.18$ at the eighth TP of the D4 sequence at $t - t_0 = 32,644$ yr. Cumulatively, this deeper DUP leads to a somewhat stronger core mass reduction than in the D4 case; the core mass at the end of the sixth TP of the D9 sequence is $m_r = 0.95539$ $M_\odot$.

5. A different He/C/O intershell abundance composition; C and O are enhanced at the expense of He. In the PDCZ of the sixth TP the mass fractions are (He/C/O) = (0.62/0.26/0.18).

Despite these differences, overshooting at the bottom of the PDCZ does not change the envelope abundance evolution qualitatively. In both cases, with and without overshooting at the bottom of the PDCZ, the DUP is efficient, and substantial amounts of primary C and O will be dredged up. Sequences of intermediate-mass and massive AGB models generally tend to converge to $\lambda = 1$ whether they start initially with $\lambda > 1$ or $\lambda < 1$ (Karakas et al. 2002). This phenomenon is already noticeable in Figure 2. Therefore, the difference in DUP efficiency is expected to decrease in later pulses. The different ^{16}O and ^{12}C abundances in the PDCZ lead to some differences in the surface evolution of the CNO elements. For a comparison, the abundance evolution of the D4 and D9 cases is shown in Figure 11 in the logarithmic square bracket units used to present abundance observations. Deeper DUP and a larger ^{12}C abundance in the PDCZ cause a larger enrichment in primary ^{14}N in the D9 case compared with the D4 case. A difference of the ^{16}O abundance of a few tenths of a dex is
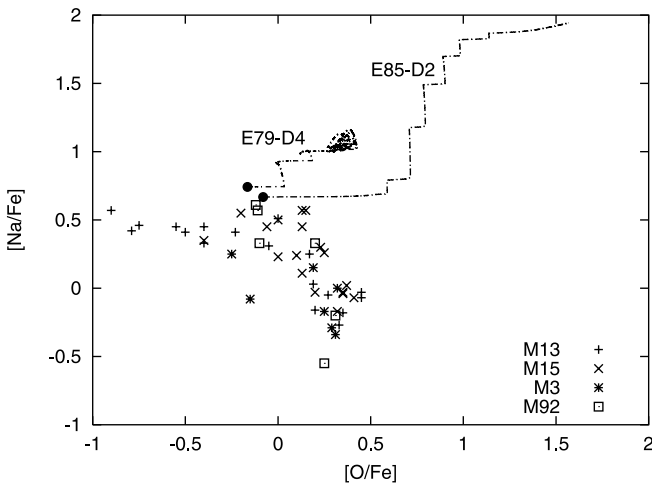

Fig. 10.—Oxygen and sodium abundances in globular cluster stars (Kraft et al. 1992, 1997; Sneden et al. 1997; Shetrone 1996) and AGB model predictions (Table 1). The 5 $M_\odot$ sequence E79-D4 has been computed without mass loss and achieves high HBB temperatures, while the 4 $M_\odot$ sequence E85-D2 has been computed with mass loss and neither oxygen nor sodium are destroyed by HBB. Both sequences start with low O and Na abundances indicated by a filled circle (see text for details). For the conversion of the model abundance mass fractions into the logarithmic abundance ratios with respect to solar, $\log {}^{16}\text{O}_\odot = -2.018$, $\log {}^{23}\text{Na}_\odot = -4.476$, and $\log {}^{56}\text{Fe}/{}^{56}\text{Fe}_\odot = -2.3$ have been used.
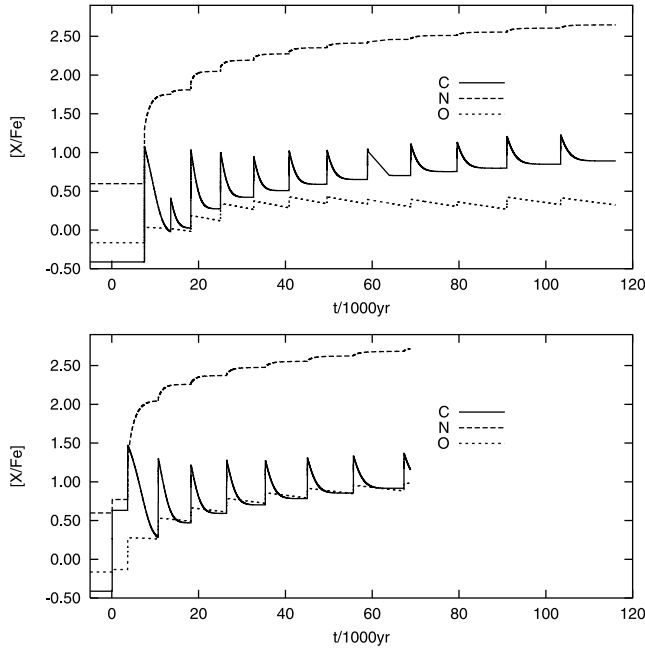
FIG. 11.—Abundance evolution in units of $[X/Fe] = \log(X/Fe) - \log(X_\odot/Fe_\odot)$, with $\log {}^{16}O_\odot = -2.018$, $\log {}^{12}C_\odot = -2.479$, $\log {}^{14}N_\odot = -2.957$, and $\log {}^{56}Fe/{}^{56}Fe_\odot = -2.3$. *Top*: Sequence D4 ($f_{PDCZ} = 0.002$, $f_{CE} = 0.016$). *Bottom*: Case D9 ($f_{PDCZ} = f_{CE} = 0.016$) (see Table 1).
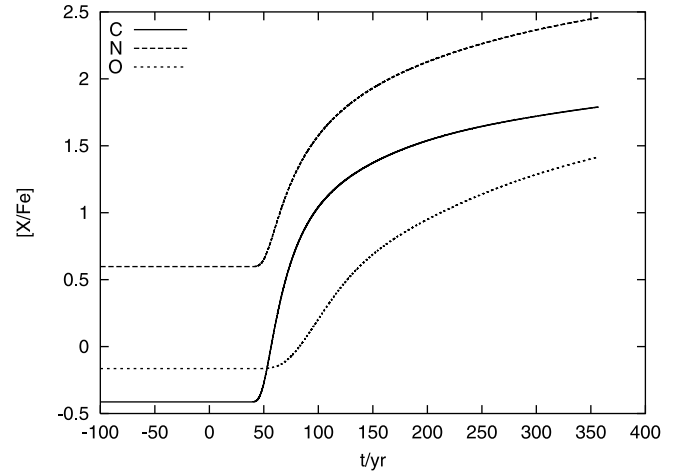

FIG. 12.—Abundance evolution in the same units as in Fig. 11 for test calculation E79-D10 after the fifth TP (see text for details); $t = 0$ yr at maximum L_{He} during the flash.

present. If many more TPs occur in this type of star, the difference of the oxygen abundance in the two cases would likely increase. However, overall the uncertainty in the model predictions of massive AGB stars does not appear to be strongly dependent on the overshooting efficiency at the bottom of the PDCZ.

Next, the influence of the exponential overshooting efficiency at the bottom of the convective envelope during the DUP phase is analyzed. A number of tests (among them E79-D10 and D11 with $f_{CE} \geq 0.032$) have been followed for several ten thousand models with small time steps during the hot DUP phase. In some cases the mixing speed has been altered too. The DUP rate was almost constant in all cases ($dm_{bce}/dt \simeq 5 \times 10^{-5} M_\odot$ yr^{-1} for E79-D10, where m_{bce} is the Lagrange coordinate of the bottom of the convective envelope) and depends somewhat on both the assumed speed and depth of the exponential overshooting. The surface abundance evolution during the ongoing hot DUP after the fifth TP (e.g., sequence E79-D10, which has been followed longest; Fig. 12) is similar to the long-term evolution over many TPs with moderate DUP (Fig. 11). However, in the latter case the N/O and the N/C ratios are larger and the C/O ratio is smaller.

When the sequence was stopped, the dredged-up mass was $\Delta M_{DUP} = 1.6 \times 10^{-2} M_\odot$, which is about 8 times the mass contained in the He-shell flash convection zone. During the hot DUP the stellar luminosity is about $\log L/L_\odot = 5$, again somewhat dependent on the details of the overshooting. With the large envelope CNO abundance enhancement, the mass loss may not be less efficient than in more metal-rich AGB stars. Assuming the mass-loss rate of Blöcker (1995) with an efficiency parameter $\eta_{BL} = 0.1$, the mass loss during this phase is of order $\dot{M} = 2 \times 10^{-3} M_\odot$ yr^{-1}. Together with an envelope mass of about $4 M_\odot$, this implies an upper limit for this evolutionary phase of $t_{DUP} < 2000$ yr, and with the DUP rate, the maximum mass of dredged-up material is $\Delta M_{DUP} \sim 0.1 M_\odot$.

We emphasize that these findings are the result of *test* calculations intended to explore the uncertainties of the model predictions. On the basis of the current models, and without good constraints on overshooting in the presence of nuclear burning, we cannot exclude that IMSs of very low metallicity end their lives in a high mass loss hot-DUP phase, possibly after a rather early TP.

5. CONCLUSION

The evolution of massive AGB stars (mainly of initial mass $5 M_\odot$ and very low metallicity, $Z = 0.0001$) has been studied in detail. Nucleosynthesis and convective mixing, including the effect of exponential overshooting, have been considered. In contrast to less massive cases and more metal-rich cases, this model predicts hot DUP, the efficient nuclear burning of hydrogen during the third DUP phase that can greatly increase the DUP efficiency. The additionally released energy feeds back into the structure evolution, leading to deeper DUP than observed in models that do not show this effect (either because strictly no mixing beyond the Schwarzschild boundary of convection is allowed or because the mass and metallicity are not in the appropriate range). In the benchmark case a DUP penetration through and beneath the He shell is found even with a rather small overshooting efficiency. For larger masses or larger overshoot efficiencies, the DUP is deeper and may eventually terminate the AGB evolution.

Our model predictions of O and Na in massive low-Z TP-AGB models is not in agreement with the trend seen in the globular clusters, and this casts doubt on the simple self-pollution scenario of globular clusters. On the other hand, AGB stars have been frequently associated with the significant overabundance of C and N in some EMP stars. EMP binaries CS 29497-030 (Sivarani et al. 2004) and LP 625-44 (Aoki et al. 2002b) show oxygen and sodium enhancements similar in magnitude to the model predictions presented here. However, the majority of C-rich EMP stars (including these two) have a larger C than N enhancement. Such an abundance pattern is incompatible with HBB in massive AGB stars, in which at all metallicities C and O are cycled efficiently into N (Figs. 11 and 12).

The EMP star HE 0024−2523 (Lucatello et al. 2003) is a post–common-envelope binary with a period of only a few days. Our models suggest that the most likely time to initiate

the common-envelope evolution should be at the time of the first TP with efficient DUP. In the 5 $M_\odot$ sequence, this is the fifth TP. During this phase the star expands temporarily very significantly (Fig. 4). The radius peaks occur at all subsequent TPs, but the maximum radius during these peaks does not significantly exceed the initial radius peak. Thus, if the common-envelope evolution has not been initiated during the preceding red giant branch or early AGB evolution, the most likely time is at the first TP with efficient DUP. We do not model the common-envelope evolution in this paper. However, it is interesting to note that the C/O ratio in the intershell is about 100 during the first TP with deep DUP (§ 4.2). During the following TPs the intershell C/O ratio decreases to ∼15 at the tenth TP. With this C/O ratio in the intershell abundance, the observed C/O ratio in HE 0024−2523 of 100 cannot be reproduced no matter how peculiar the burning and mixing induced by the common-envelope evolution may be. However, HE 0024−2523 is highly s-process–enhanced, and it is not clear how this can be explained without a succession of neutron exposures in many subsequent TP cycles. This example shows that the s-process in AGB stars of very low metallicity is not yet very well understood.

Our calculations confirm the previously found trend that both a lower metallicity and a larger core mass increase the DUP efficiency in terms of the DUP parameter λ (e.g., Boothroyd & Sackmann 1988). Marigo (2001) and Marigo, Girardi, & Bressan (1999) found semiempirically that low-mass and moderately metal-deficient AGB stars should already have a substantial DUP parameter of $\lambda \sim 0.5$. The fact that our models show larger λ is generally consistent with this trend. We have shown that efficient DUP can be found even under the assumption of small overshooting efficiency and that a high numerical resolution is required for DUP predictions.

REFERENCES

Alexander, D., & Ferguson, J. 1994, ApJ, 437, 879
Alibés, A., Labay, J., & Canal, R. 2001, A&A, 370, 1103
Anders, E., & Grevesse, N. 1989, Geochim. Cosmochim. Acta, 53, 197
Angulo, C., et al. 1999, Nucl. Phys. A, 656, 3
Aoki, W., Ryan, S. G., Norris, J. E., Beers, T. C., Ando, H., & Tsangarides, S. 2002a, ApJ, 580, 1149
Aoki, W., et al. 2001, ApJ, 561, 346
———. 2002b, PASJ, 54, 427
Blöcker, T. 1995, A&A, 297, 727
Boothroyd, A. I., & Sackmann, I.-J. 1988, ApJ, 328, 671
Busso, M., Gallino, R., Lambert, D. L., Travaglio, C., & Smith, V. V. 2001, ApJ, 557, 802
Busso, M., Gallino, R., & Wasserburg, G. J. 1999, ARA&A, 37, 239
Carney, B. W. 1996, PASP, 108, 900
Caughlan, G. R., & Fowler, W. A. 1988, At. Data Nucl. Data Tables, 40, 283
Chieffi, A., Dominguez, I., Limongi, M., & Straniero, O. 2001, ApJ, 554, 1159
Cottrell, P. L., & Da Costa, G. S. 1981, ApJ, 245, L79
Denissenkov, P. A., & Herwig, F. 2003, ApJ, 590, L99
Denissenkov, P. A., Weiss, A., & Wagenhuber, J. 1997, A&A, 320, 115
Dreizler, S., Werner, K., Heber, U., & Engels, D. 1996, A&A, 309, 820
El Eid, M., & Champagne, A. E. 1995, ApJ, 451, 298
Gallino, R., Arlandini, C., Busso, M., Lugaro, M., Travaglio, C., Straniero, O., Chieffi, A., & Limongi, M. 1998, ApJ, 497, 388
Girardi, L., Bressan, A., Chiosi, C., Bertelli, G., & Nasi, E. 1996, A&AS, 117, 113
Goriely, S., & Mowlavi, N. 2000, A&A, 362, 599
Gratton, R. G., Sneden, C., Carretta, E., & Bragaglia, A. 2000, A&A, 354, 169
Gratton, R. G., et al. 2001, A&A, 369, 87
Grevesse, N., & Noels, A. 1993, in Origin and Evolution of the Elements, ed. N. Pratzo, E. Vangioni-Flam, & M. Casse (Cambridge: Cambridge Univ. Press), 15
Grevesse, N., & Sauval, A. J. 1998, Space Sci. Rev., 85, 161
Herwig, F. 2000, A&A, 360, 952
———. 2001, ApJ, 554, L71
———. 2003, in IAU Symp. 209, Planetary Nebulae: Their Evolution and Role in the Universe, ed. S. Kwok, M. Dopita, & R. Sutherland (San Francisco: ASP), 61
Herwig, F., Blöcker, T., Langer, N., & Driebe, T. 1999, A&A, 349, L5
Herwig, F., Blöcker, T., Schönberner, D., & El Eid, M. F. 1997, A&A, 324, L81
Herwig, F., Langer, N., & Lugaro, M. 2003, ApJ, 593, 1056
Iben, Jr., I., & Renzini, A. 1983, ARA&A, 21, 271

Iglesias, C. A., & Rogers, F. J. 1996, ApJ, 464, 943
Karakas, A. I., Lattanzio, J. C., & Pols, O. R. 2002, Publ. Astron. Soc. Australia, 19, 515
Koesterke, L., & Hamann, W. R. 1997, A&A, 320, 91
Kraft, R. P., Sneden, C., Langer, G. E., & Prosser, C. F. 1992, AJ, 104, 645
Kraft, R. P., Sneden, C., Smith, G. H., Shetrone, M. D., Langer, G. E., & Pilachowski, C. A. 1997, AJ, 113, 279
Lattanzio, J. 1992, Publ. Astron. Soc. Australia, 10, 99
Lattanzio, J., & Forestini, M. 1999, in IAU Symp. 191, Asymptotic Giant Branch Stars, ed. T. Le Bertre, A. Lèbre, & C. Waelkens (San Francisco: ASP), 31
Lucatello, S., Gratton, R., Cohen, J. G., Beers, T. C., Christlieb, N., Carretta, E., & Ramirez, S. 2003, AJ, 125, 875
Lugaro, M., Herwig, F., Lattanzio, J. C., Gallino, R., & Straniero, O. 2003, ApJ, 586, 1305
Marigo, P. 2001, A&A, 370, 194
Marigo, P., Girardi, L., & Bressan, A. 1999, A&A, 344, 123
Miksa, S., Deetjen, J. L., Dreizler, S., Kruk, J. W., Rauch, T., & Werner, K. 2002, A&A, 389, 953
Morgan, H. L., & Edmunds, M. G. 2003, MNRAS, 343, 427
Mowlavi, N. 1999, A&A, 344, 617
Nicolussi, G. K., Pellin, M. J., Lewis, R. S., Davis, A. M., Clayton, R. N., & Amari, S. 1998, Phys. Rev. Lett., 81, 3583
Nissen, P. E., & Schuster, W. J. 1997, A&A, 326, 751
Pagel, B. E., & Portinari, L. 1998, MNRAS, 298, 747
Pettini, M., Ellison, S. L., Bergeron, J., & Petitjean, P. 2002, A&A, 391, 21
Prochaska, J. X., Henry, R. B. C., O'Meara, J. M., Tytler, D., Wolfe, A. M., Kirkman, D., Lubin, D., & Suzuki, N. 2002, PASP, 114, 933
Reddy, B. E., Lambert, D. L., Gonzalez, G., & Yong, D. 2002, ApJ, 564, 482
Schönberner, D. 1979, A&A, 79, 108
Shetrone, M. D. 1996, AJ, 112, 2639
Siess, L., Livio, M., & Lattanzio, J. 2002, ApJ, 570, 329
Sivarani, T., et al. 2004, A&A, in press   Q3
Sneden, C., Kraft, R. P., Shetrone, M. D., Smith, G. H., Langer, G. E., & Prosser, C. F. 1997, AJ, 114, 1964
Timmes, F. X., Woosley, S. E., & Weaver, T. A. 1995, ApJS, 98, 617
van Winckel, H., & Reyniers, M. 2000, A&A, 354, 135
Ventura, P., D'Antona, F., & Mazzitelli, I. 2002, A&A, 393, 215
Woosley, S. E., & Weaver, T. A. 1995, ApJS, 101, 181
Zinner, E. 1998, Annu. Rev. Earth Planet. Sci., 26, 147

AUTHOR QUERIES

Q1 Auth: Your article has been edited for grammar, consistency, and to conform to ApJ journal style (see Instructions to Authors). To expedite publication, we generally do not query every routine grammatical and style change made to a manuscript, although all substantive changes have been noted. Please review the article carefully. Note that we may be unable to make changes that conflict with journal style, obscure meaning, or create grammatical or other problems. It is ApJ style to have no titles on figures. Any text appearing at the top of a figure, with the exception of an axis label, has been removed and incorporated into the legend. Also note that article proofs via PDF do not show corrections that will have been made by the typesetter's proofreader, which generally include corrections of errors of page layout, figure placement, and spacing and font mistakes; feel free to mark any errors you notice in these areas. **When sending us your corrections, if you are writing them by hand, please print clearly. If sending a fax, please do not write too close to the margins of the page, since these are often cut off in fax transmission. Finally, please note that a delayed, incomplete, or illegible response may delay the publication of your article while we contact you.**

Q2 Auth: I have renumbered Figs. 8 and 7 as Figs. 7 and 8 and inserted the sentence beginning ''In Figure 7 the energy generation'', per your email of Feb 5. Please ensure that all changes are correct.

Q3 Auth: In-press year has been changed from 2003.